Hierarchical microstructure for improved fatigue properties in a eutectic high entropy alloy

Shivakant Shukla, Tianhao Wang, Shomari Cotton, Rajiv S. Mishra*

Center for Friction Stir Processing and Advanced Materials Manufacturing Processing Institute, Department of Materials Science and Engineering,

University of North Texas, Denton, TX 76203, USA

*Corresponding author: email ID — Rajiv.Mishra@unt.edu

Abstract

Microstructural hierarchy can enable enhanced properties in high entropy alloys. A unique microstructure was observed in 50% cold-rolled and heat-treated eutectic high-entropy alloy (EHEA). Formation of recrystallized FCC grains and B2 precipitates in FCC lamellae with different microstructural length scale constitute the hierarchy in cold-rolled and heat-treated EHEA. Monotonic loading and high cycle fatigue properties of both microstructures were compared. In as-cast microstructure, the fatigue crack originated in FCC lamellae with the formation of persistent slip bands. The B2 precipitates in cold-rolled and heat-treated alloy delayed the crack initiation and improved fatigue properties.

Keywords: - Eutectic high-entropy alloys; Hierarchical microstructure; Fatigue; Crack initiation; Persistent slip bands (PSBs).

Since the discovery of copper in 9000 BC, humankind has tried to improve the strength of metals in numerous ways. Improvement in strength has been largely due to grain refinement, work-hardening and alloying or any other combinations of these mechanism [1,2]. A new class of material, known as high entropy alloys (HEAs), has drawn significant attraction in recent years. Some of the initial literatures have defined HEAs as “single phase solid solutions composed of five or more principal elements, generally in equimolar quantities” [3,4]. Although the definition emphasized “single phase”, the ever-expanding research on this topic has led to various multi-

phase HEAs and hence other terms like multi-principal elemental alloys (MPEAs) and complex concentrated alloys (CCAs) have been coined [5]. With their vast range of compositions, HEAs possess many remarkable properties such as excellent tensile properties and hardness [6,7], good high-temperature mechanical as well as refractory properties [7,8], and excellent cryogenic fracture resistance [9,10].

Cumulative damage of materials due to cyclic loading is known as fatigue, which is a crucial property for any structural component as in-service alloys are generally subjected to a non-monotonic loading. Only a few studies have focused on the fatigue behavior of HEAs. Hemphill et al. [11] investigated the fatigue behavior of $Al_{0.5}CoCrFeCuNi$ in cold-rolled and annealed condition which exhibited high fatigue endurance limit. A large variance in the fatigue limit and scatter was attributed to the aluminum oxide particles and cracks during casting and rolling. Also, in another study on the same alloy, Tang et al. [12] reported on the effect of impurities and processing route on the fatigue properties. They also investigated the effect of nano-twins on fatigue properties, concluding that nano-twinning behavior resulted in a better fatigue life and high fatigue strength of about 383 MPa. A recent study by Niendorf et al. [13] focused on the low cycle fatigue properties of $Fe_{50}Mn_{30}Co_{10}Cr_{10}$ HEA alloy in rolled and annealed condition with two different grain sizes. They reported a completely different deformation mechanism in $Fe_{50}Mn_{30}Co_{10}Cr_{10}$ HEA when compared with high-Mn twinning-induced plasticity (TWIP)/transformed-induced plasticity (TRIP) steel. Apart from the above-mentioned studies on two-phase HEAs, some single phase HEAs were also subjected to fatigue testing. Thurston et al. [14] studied the effect of temperature on the fatigue crack growth of single phase CrMnFeCoNi HEA in rotary swaged and recrystallized condition.

Microstructure containing hierarchical features can be engineered to obtain favorable properties [15]. In past, such a process has been utilized to enhance superplastic properties of titanium alloys [16] and aluminum alloys [17]. Also, in Ni based superalloys, hierarchical microstructure develops during heat-treatment [18] and provide key benefits to balance of properties. Given the complexity of physical metallurgy in HEAs, they provide excellent opportunity for building complex microstructure to get desired combination of properties. Studies of many multiphase HEAs have established that an excellent combination of strength and ductility can be achieved by blending relatively harder and softer phases. Eutectic HEAs (EHEA), with a combination of

hard BCC phase and soft FCC phase in lamellar morphology, have excellent castabilty in addition to good mechanical properties in as-cast condition [19]. Furthermore, 90% cold-rolled and annealed microstructure has an excellent combination of strength and ductility [20,21]. A recent study on the thermomechanical processing of EHEA shows that lamellar microstructure can be retained [22]. Although high-density dislocation network and disordering of $L1_2$ phase have been observed, B2 phase ordering was still present in the 50% rolled microstructure. Furthermore, Cr-rich disordered BCC nano-precipitates have been observed in the BCC(B2) phase. These observations point towards three distinct features of EHEA. (i) lamellar morphology, (ii) semi-coherent interface between BCC (B2) and FCC ($L1_2$) phases and (iii) intra-lamellar features within the BCC and FCC phases. Hence, it provides an opportunity to understand the effect of all these features on fatigue behavior of EHEA.

Commercially pure elements of Al (99.9 wt%), Co (99.9 wt %), Ni (99.9 wt %), Cr and Fe (99.5 - 99.6 wt %) were used in the casting of $AlCoCrFeNi_{2.1}$ (in atomic ratio). Two conditions were chosen for the present study – (i) EHEA in as-cast condition, hereafter named $EHEA_c$ and (ii) as-cast EHEA rolled to 50% of initial thickness and heat-treated at 700°C for 12 hours, hereafter named $EHEA_w$. The mini-tensile and mini-fatigue samples were prepared via CNC machine. Samples were mechanically polished to a surface roughness of 0.05 μm using colloidal silica to minimize any surface flaw. Gage length of the mini-tensile samples was ~5 mm with width of ~1 mm, and thickness of ~1.1 mm. Mini-tensile testing was carried out on a custom build computer-controlled mini-tensile tester at an initial strain rate of 10^{-3} s^{-1}. Bending fatigue testing was performed using a custom-made tabletop mini-fatigue testing machine. Thickness of mini-fatigue samples was ~ 1 mm with an effective gage length of ~ 3.05 mm and a taper angle of 28°. The details regarding the geometry of fatigue samples and the description of the bending fatigue setup can be found in [23]. All samples were tested at 20 Hz frequency and stress ratio (R) of -1. Backscattered electron (BSE) imaging was done on FEI Nova NanoSEM 230, with an 18 kV accelerating voltage. The EBSD analysis was executed using SL Digiview III electron backscatter diffraction (EBSD) detector on FEI Nova NanoSEM 230, with a 20 kV accelerating voltage and a step size of 40 nm. For electron microscopy, samples were polished down to a surface finish of 0.02 μm.

Figs. 1 (a-d) show the microstructure of the as-cast $AlCoCrFeNi_{2.1}$ ($EHEA_c$). The initial

microstructure is composed of lamellae of FCC($L1_2$) and BCC(B2). The EBSD analysis (Figs 1(b, c)) reveals the FCC ($L1_2$) fraction to be around 71% while BCC(B2) to be around 29%. Spacing between each FCC lamellae is around 0.70 μm and spacing between BCC lamellae is around 1.3 μm. Cr-rich precipitates have been marked with an arrow in high-resolution BSE image (Fig. 1 (d)). Microstructure and EBSD images of $EHEA_w$ (after cold rolling to 50% and heat treatment at 700°C for 12 hours) are shown in Figs. 1 (e-h). For $EHEA_w$ the fraction of FCC ($L1_2$) is around 68% and BCC(B2) around 32% respectively. The hierarchy in $EHEA_w$ is characterized by four distinct microstructural features- (i) lamellar FCC region (ii) deformed and subsequent recrystallized FCC phase (Fig. 1 (f-g)) with various BCC/B2 phases having different morphologies (Fig. 1 (h)), (iii) lamellar BCC(B2) with Cr rich precipitates and (iv) recrystallized BCC phase. Details regarding the precipitation mechanism of B2 phase inside FCC matrix via cold rolling and heat-treatment can be found elsewhere [24]. The recrystallized FCC phase and BCC phase within the FCC lamellae can be attributed to the cold-rolling and subsequent heat treatment process.

Fig. 2 (a) depicts a tensile plot for both $EHEA_c$ and $EHEA_w$ tested at an initial strain rate of 10^{-3} s^{-1}. $EHEA_c$ exhibits a yield strength (YS) of ~746 MPa and ultimate tensile strength (UTS) of ~1057 MPa with a uniform elongation of ~8%. Except for the % elongation value, all the other values are in accordance with the earlier studies [19,20,21]. The properties of as-cast materials are highly dependent on the the casting conditions and hence the low ductilty. The variance of the quasi-static properties of $EHEA_c$ from literature can be attributed to the size of ingots, cooling rate, etc. Besides, the as-cast microstructure features (i.e. lamellae size, spacing and fraction of BCC to FCC phases etc.) are also responcible for the resultant mechanical properties. In comparison, the YS and UTS of $EHEA_w$ are substantially enhanced to a value of ~1110 MPa and ~1340 MPa with a total elongation of ~10%. Fig. 2 (b) illustrates the work hardening response of both microstructures as a function of the strain. Clearly evident is the difference in stage B (highlighted by red and blue shaded regions Fig. 2 (b)) of both microstructures. Since stage B is generally associated with twinning mediated plasticity, it is apparent that $EHEA_w$, with a combination of recrystallized FCC grains and higher fraction of annealing twin boundaries (Figs. 1 (f-h)), is expected to exhibit an almost zero slope in stage B causing sustained strain-hardening rate. An earlier investigation by Wani et al. [20] on 90% cold-rolled and heat treated EHEA reported the formation of ultrafine grained (UFG) microstructure with YS and UTS

values of 1100 MPa and 1200 MPa, respectively. The current study achieves even higher strength and improved work-hardening without the loss of ductility. The microstructural hierarchy is responsible for enhanced properties of $EHEA_w$ when compared with UFG EHEA as different length scale microstructural features such as B2 precipitates, with the combination of recrystallized features and lamellae of FCC and BCC phases provide better monotonic load bearing capacity.

Fully reversible bending fatigue properties of both $EHEA_c$ and $EHEA_w$ in the high cycle fatigue (HCF) regime is shown in Fig 2 (c) in form of typical S-N curves. It is clearly evident that the cyclic loading behavior of $EHEA_w$ is better than that of $EHEA_c$. Fatigue runout, i.e. the stress at which sample does not fail till 10^7 cycles, is also improved from ~ 390 MPa for $EHEA_c$ to ~ 500 MPa for $EHEA_w$. The normalized stress amplitude vs number of cycles to failure curves for both microstructures (Fig. 2 (d)) also underscore these findings.

The overall fatigue life (N_f) of a material can be divided into two parts: - (a) number of cycles for crack initiation (N_i) and (b) number of cycles for crack propagation (N_p).

$$N_f = N_i + N_p$$

Various studies indicate that primary cause of crack initiation is the localization of strain. This strain localization is due to the fact that slip during forward and reverse loading is not completely reversible. The subsequent loading results in additional dislocation nucleation which, by a process of climb, cross-slip or looping process, forms a low energy pathway [25]. These low energy pathways present an easy route for further dislocation motion resulting in the formation of persistent slip bands (PSBs). In many cases either the crack initiates along these PSBs or due to the interaction of PSBs with grain boundary or twin boundary [26,27,28]. Nevertheless, crack nucleated due to PSBs along the preferred crystallographic direction is known as microscopically small fatigue crack, and tends to grow either intragranularly or transgranularly depending on the local microstructure. In the fully reversible bending fatigue test, a plot of the variation of stress amplitude as a function of the number of cycles can help identify the initiation of crack and its growth to a microscopically small crack [29]. Fig. 3 (a) shows the crack initiation period (N_i) for both $EHEA_c$ and $EHEA_w$ samples tested at a stress amplitude of 600 MPa and 700 MPa, respectively. While crack initiation life for $EHEA_c$ is little above 30,000 cycles, the same for

$EHEA_w$ jumps to a value of about 85,000 cycles even at a higher stress. This leads to an important conclusion that by introducing hierarchical features into the microstructure, crack initiation period (N_i) can be delayed to a substantial degree.

In order to explore the reason behind the delayed crack initiation, microstructural investigation after cyclic loading of $EHEA_c$ and $EHEA_w$ was carried out. Fig. 3 (b) shows several slip traces and crack formation sites in FCC phase of $EHEA_c$. Multiple slip bands formation was observed during cyclic loading. Fig. 3 (c) shows the EBSD plot of one such region with PSBs formation along two different orientation {111} planes. Cracks are generally formed along these slip bands. Noticeably, no slip activity was observed in BCC lamellar region at early stages of cyclic loading even at high-stress amplitude. After encountering the FCC/BCC phase boundary, crack generally propagated along the phase boundary as lamellar phase boundaries represent an easier path for crack propagation. In some cases when the microscopically small crack has grown to physically small crack, the stress intensity at crack tip is large enough to penetrate the BCC phase, as shown in Fig. 3 (d), and hence crack bifurcates and travels into BCC phase in addition to the primary propagation direction. In many titanium alloys and cast iron with lamellar microstructure, such behavior of crack propagation has been known to improve fatigue crack propagation life [30,31,32]. On the other hand, in case of $EHEA_w$, with a variety of B2 precipitates in the FCC lamellae a clear path for PSB formation has hindered Figs. 3(e-f) which leads to a delay in crack nucleation.

To better understand the underlying mechanism of delay in the crack initiation, a schematic has been shown in Fig. 4. The $AlCoCrFeNi_{2.1}$ HEA has low stacking fault energy (SFE) [22]. Low SFE can lead to formation of planar slip for deformation during cyclic loading [27]. Fig. 4 (a) presents an example of two slip system in FCC lattice along which the deformation can occur (shown by green and red arrows). The primary slip system is decided by its proximity to the shear direction. In case of $EHEA_c$ with no precipitates in FCC matrix, the deformation proceeds along the primary slip system until it reaches the phase boundary (BCC/FCC lamella) and results in crack nucleation along phase boundary or slip transfer to BCC phase (Fig 4 (b)). However, in the case of $EHEA_w$, apart from recrystallized FCC grains with twin boundaries and high angle grain boundaries, the FCC lamellae contains recrystallized B2 precipitates of different morphology and scales. These B2 precipitates create obstacles to the low energy pathways. Any

barrier in these pathways will also hinder the propagation of PSBs resulting in the activation of other slip systems as shown in Fig. 4 (c). Furthermore, these newly activated slip systems promote the formation of new PSBs along which the crack can propagate.

It is also imperative to mention that although no slip traces or PSBs were observed in the BCC(B2) lamellae during cyclic loading, slip transfer from FCC to BCC can be seen in BSE images in Fig. 3. The absence of slip trace on BCC(B2) lamellar phase can be justified by the presence of strong lattice friction in conventional BCC alloys. In BCC materials, strong lattice friction forces screw dislocations to move in a straight line forming long screw dislocation structure leaving only the edge dislocation to participate in the glide process [33,34]. In low plastic strain regime such as HCF testing in the current study, cyclic slip occurs mainly via quasi-reversible glide of mobile edge dislocations and hence very low cyclic hardening occurs. Therefore, fatigued BCC matrix structure does not contain dipole edge dislocation which explains the reason for lack of PSBs. In addition, Gao et al. [22] reported that during monotonic loading, Cr-rich precipitates in BCC(B2) lamellae impinges the dislocation motion. Even though the experimental observation in this study strongly substantiate the above-mentioned hypothesis, further study is required to fully understand the inherent micro-mechanism during cyclic loading in BBC(B2) phase in EHEA.

Summarizing, a unique variant of eutectic high entropy alloy with hierarchical microstructure ($EHEA_w$) was prepared via conventional rolling and heat-treatment of as-cast EHEA. The cyclic loading properties of both as-cast EHEA and $EHEA_w$ were compared in the high cycle fatigue regime. The following conclusions were made:

- The monotonic load bearing capacity of $EHEA_w$ is considerably higher than the same of as-cast EHEA. A unique microstructure consisting of FCC($L1_2$) lamellae, recrystallized FCC grains with high angle grain boundaries and twin boundaries, BCC(B2) precipitates inside FCC matrix, and BCC(B2) lamellae with Cr-rich precipitates was formed.
- PSB formation in FCC($L1_2$) lamellae was the main reason for crack initiation in $EHEA_c$.
- Fatigue crack initiation of $EHEA_w$ was delayed due to (BCC)B2 precipitates which hinder the path of PSBs.

Authors acknowledge the support of National Science Foundation (NSF) grant 1435810. Help of

Mathew Carl and Nathan Ley for rolling the samples at University of North Texas is also appreciated.

Reference

[1] N.F. Mott, The London, Edinburgh, and Dublin Philosophical Magazine and Journal of Science. 43 (1952) 1151.

[2] B. Gwalani, V. Soni, M. Lee, S.A. Mantri, Y. Ren, R. Banerjee, Mater Des. 121 (2017) 254.

[3] B.S. Murty, J. Yeh, S. Ranganathan, High-Entropy Alloys, Butterworth-Heinemann, 2014.

[4] M. Tsai, J. Yeh, Materials Research Letters. 2 (2014) 107.

[5] D.B. Miracle, O.N. Senkov, Acta Materialia. 122 (2017) 448.

[6] J. He, H. Wang, H. Huang, X. Xu, M. Chen, Y. Wu, X. Liu, T. Nieh, K. An, Z. Lu, Acta Materialia. 102 (2016) 187.

[7] O. Senkov, G. Wilks, J. Scott, D. Miracle, Intermetallics. 19 (2011) 698.

[8] O.N. Senkov, G.B. Wilks, D.B. Miracle, C.P. Chuang, P.K. Liaw, Intermetallics. 18 (2010) 1758.

[9] B. Gludovatz, A. Hohenwarter, K.V. Thurston, H. Bei, Z. Wu, E.P. George, R.O. Ritchie, Nature communications. 7 (2016).

[10] B. Gludovatz, A. Hohenwarter, D. Catoor, E.H. Chang, E.P. George, R.O. Ritchie, Science. 345 (2014) 1153.

[11] M.A. Hemphill, T. Yuan, G. Wang, J. Yeh, C. Tsai, A. Chuang, P. Liaw, Acta Materialia. 60 (2012) 5723.

[12] Z. Tang, T. Yuan, C. Tsai, J. Yeh, C.D. Lundin, P.K. Liaw, Acta Materialia. 99 (2015) 247.

[13] T. Niendorf, T. Wegener, Z. Li, D. Raabe, Scr. Mater. 143 (2018) 63.

[14] K.V. Thurston, B. Gludovatz, A. Hohenwarter, G. Laplanche, E.P. George, R.O. Ritchie, Intermetallics. 88 (2017) 65.

[15] K.K. Sankaran, R.S. Mishra, Metallurgy and Design of Alloys with Hierarchical Microstructures, Elsevier, 2017.

[16] R.S. Mishra, V. Stolyarov, C. Echer, R. Valiev, A. Mukherjee, Materials Science and Engineering: A. 298 (2001) 44.

[17] Z. Ma, F. Liu, R. Mishra, Acta materialia. 58 (2010) 4693.

[18] F. Vogel, N. Wanderka, Z. Balogh, M. Ibrahim, P. Stender, G. Schmitz, J. Banhart, Nature

communications. 4 (2013) 2955.

[19] Y. Lu, Y. Dong, S. Guo, L. Jiang, H. Kang, T. Wang, B. Wen, Z. Wang, J. Jie, Z. Cao, Scientific reports. 4 (2014) 6200.

[20] I. Wani, T. Bhattacharjee, S. Sheikh, Y. Lu, S. Chatterjee, P.P. Bhattacharjee, S. Guo, N. Tsuji, Materials Research Letters. 4 (2016) 174.

[21] I.S. Wani, T. Bhattacharjee, S. Sheikh, P.P. Bhattacharjee, S. Guo, N. Tsuji, Materials Science and Engineering: A. 675 (2016) 99.

[22] X. Gao, Y. Lu, B. Zhang, N. Liang, G. Wu, G. Sha, J. Liu, Y. Zhao, Acta Materialia. 141 (2017) 59.

[23] P. De, C. Obermark, R. Mishra, Journal of Testing and Evaluation. 36 (2008) 402.

[24] D. Choudhuri, S. Shukla, W.B. Green, B. Gwalani, V. Ageh, R. Banerjee, R.S. Mishra, Materials Research Letters. 6 (2018) 171.

[25] W. Baxter, oAFOM.K.7-I685. (1987) 43.

[26] P. Lukï, L. Kunz, Philosophical magazine. 84 (2004) 317.

[27] M.D. Sangid, Int. J. Fatigue. 57 (2013) 58.

[28] I. Roth, M. Kübbeler, U. Krupp, H. Christ, C. Fritzen, Procedia Engineering. 2 (2010) 941.

[29] P. Nelaturu, S. Jana, R.S. Mishra, G. Grant, B.E. Carlson, Materials Science and Engineering: A. (2018).

[30] J. Yang, H. Li, D. Hu, M. Dixon, Intermetallics. 45 (2014) 89.

[31] R.K. Nalla, R.O. Ritchie, B.L. Boyce, J.P. Campbell, J.O. Peters, Metallurgical and Materials Transactions A. 33 (2002) 899.

[32] K. Tokaji, T. Horie, Y. Enomoto, Int. J. Fatigue. 28 (2006) 281.

[33] T. Magnin, C. Ramade, J. Lepinoux, L. Kubin, Materials Science and Engineering: A. 118 (1989) 41.

[34] H. Mughrabi, Metallurgical and Materials Transactions B. 40 (2009) 431.

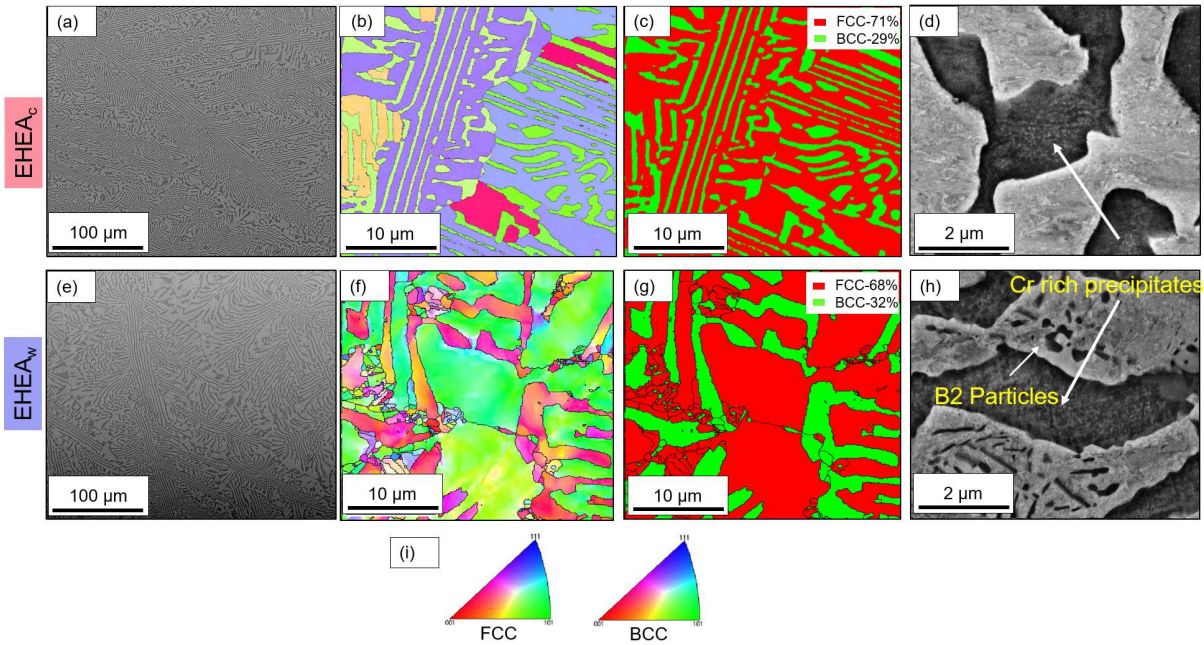

Fig. 1. Initial microstructure of EHEA with (a) BSE image of EHEAc, (b) and (c) EBSD and phase map of $EHEA_c$, (d) high magnification BSE image of $EHEA_c$, (e) BSE image of $EHEA_w$, (f) and (g) EBSD and phase map of $EHEA_w$, (h) high magnification BSE of $EHEA_w$, and (i) inverse pole figure legend for FCC and BCC phases.

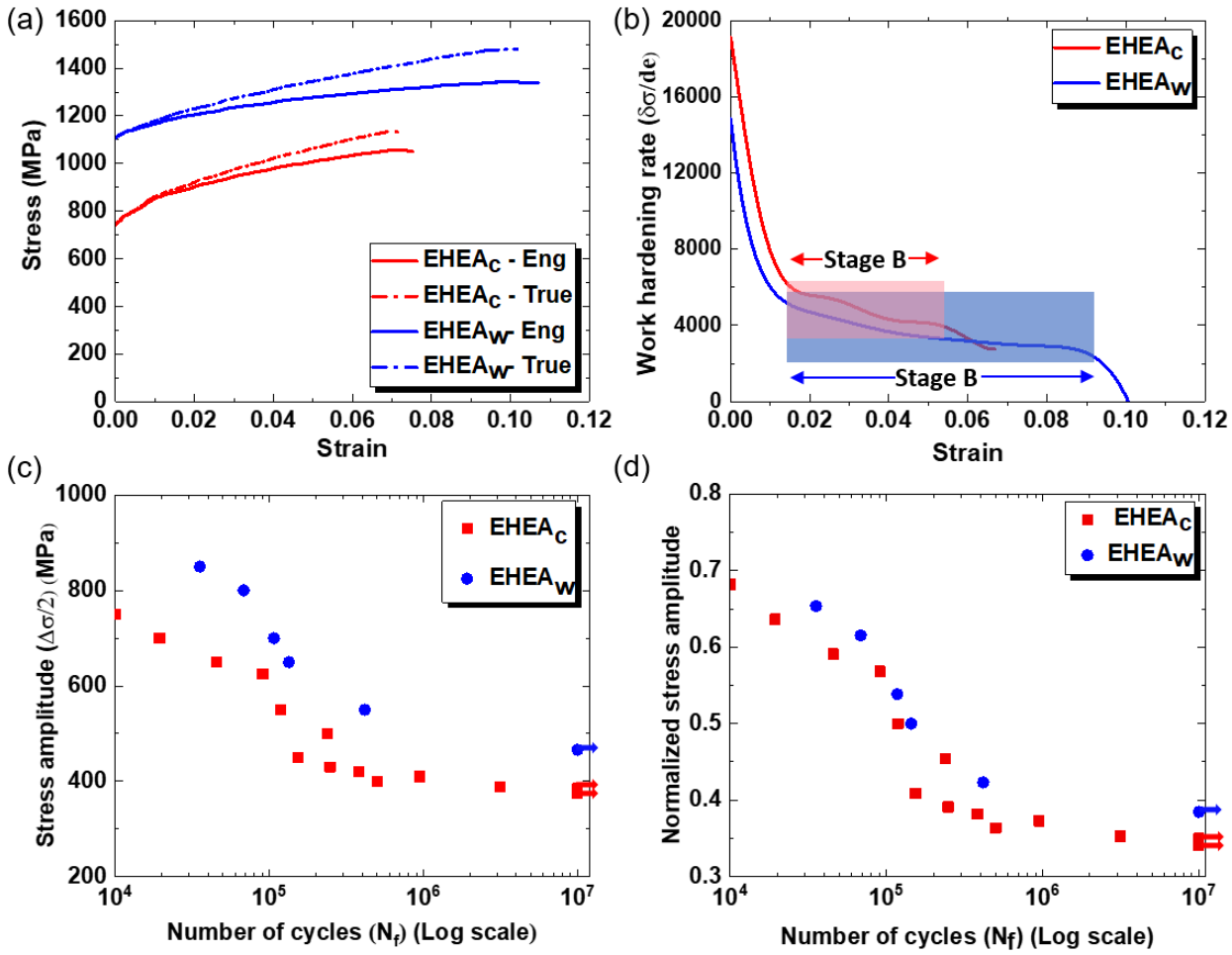

Fig. 2. (a) Engineering and true stress-strain curves, (b) strain-hardening curves, (c) stress vs number of cycles to failure and (d) UTS normalized stress vs number of cycles to failure (S-N) curves for both $EHEA_c$ (red) and $EHEA_w$ (blue).

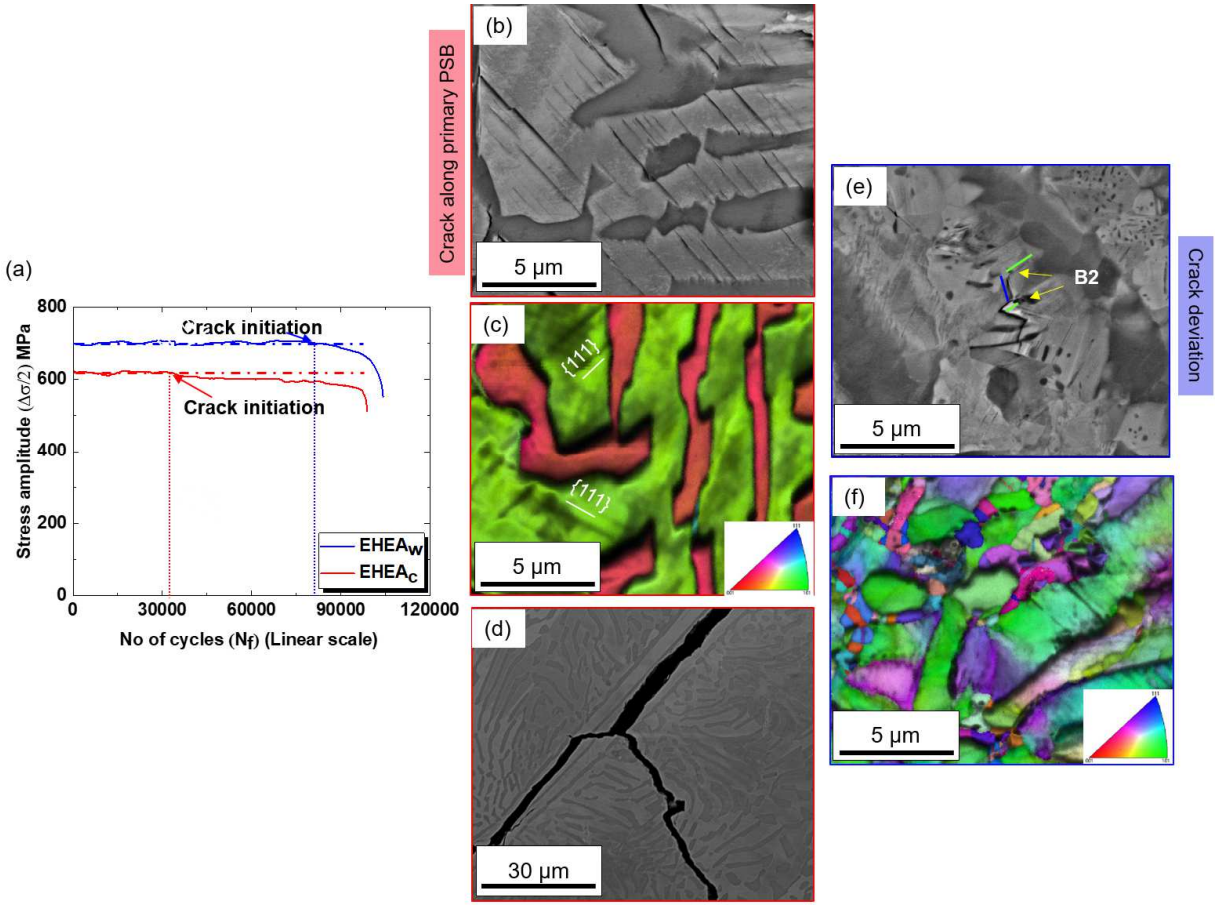

Fig. 3. (a) A plot showing crack initiation stage and total fatigue life, (b) BSE image of PSBs and cracks in EHEA$_c$, (c) EBSD image of PSBs on {111} type plane for EHEA$_c$, (d) BSE image of crack bifurcation in EHEA$_c$, (e) BSE image of EHEA$_w$ showing PSBs and crack deviation by B2 precipitate (shown by yellow arrows.) and (f) EBSD image of fatigued EHEA$_w$.

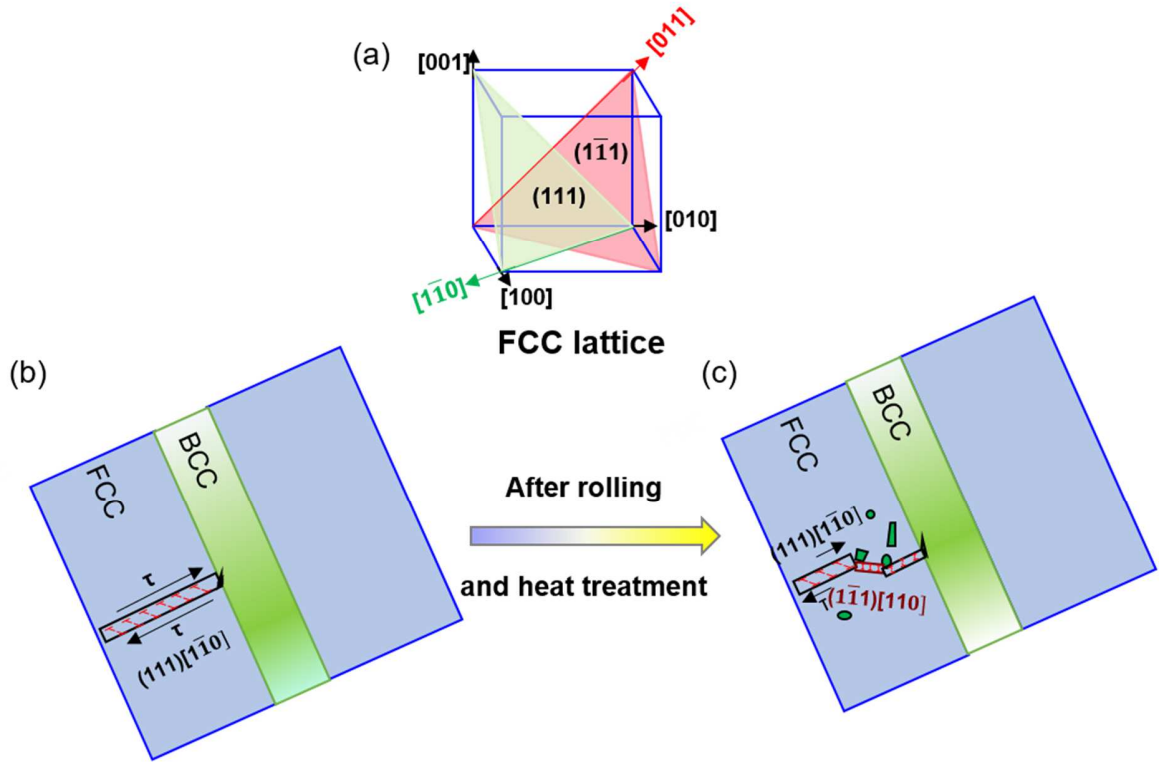

Fig. 4. Schematic illustration of crack delay with (a) two primary slip system in FCC lattice (shown by red and green arrow), (b) crack initiation in $EHEA_c$, and (c) PSB and crack deflection in $EHEA_w$ at B2 particles.

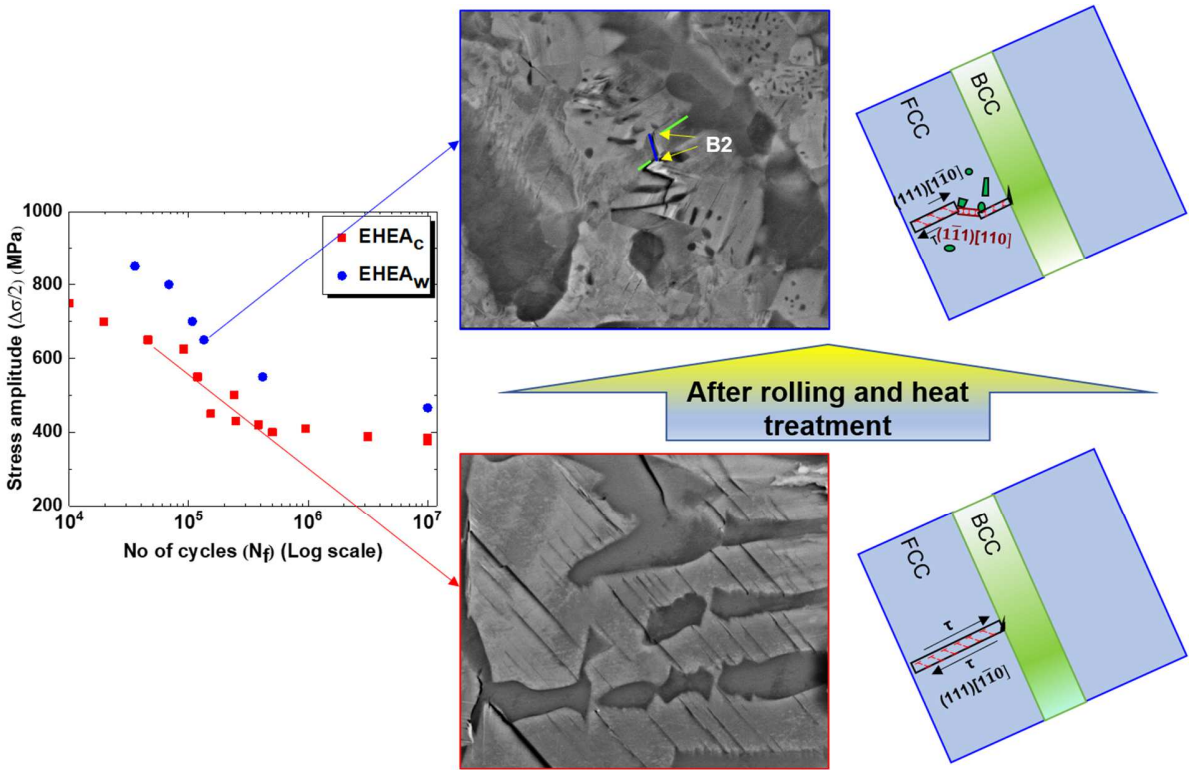
Stress amplitude (Δσ/2) (MPa)
1000
800
600
400
200
10^4
10^5
10^6
10^7
No of cycles (Nf) (Log scale)
EHEA_C
EHEA_W
B2
FCC
BCC
(111)[1̄10]
(1̄11)[110]
After rolling and heat treatment
FCC
BCC
τ
τ
(111)[1̄10]